Bulletin of the Seismological Society of America, Vol. 93, No. 6, pp. 2459–2476, December 2003

The 1999 Hector Mine Earthquake: The Dynamics of a Branched Fault System

by David D. Oglesby, Steven M. Day, Yong-Gang Li, and John E. Vidale

Abstract The 1999 *M* 7.1 Hector Mine earthquake ruptured a complex fault system with a branched structure in the north. This fault geometry and slip pattern presents a puzzle, because the northwest branch of this system should be in the stress shadow of the north branch, upon which nucleation likely took place. Through 3D dynamic models of this event, we show that the ability of rupture to propagate to the northwest branch most likely depends on the fact that rupture did not proceed to the surface on the north branch. This slip pattern leads to part of the northwest branch being brought above its failure stress and to subsequent rupture propagation and slip occurring on that branch. A similar effect can be seen in the case in which rupture is constrained not to propagate to the base of the north branch. Models with slip over the entire north branch do not produce rupture propagation and slip on the northwest branch. The results are robust with respect to details of the prestress pattern and hypocenter location. Large heterogeneity over small length scales in the final stress pattern is a natural product of the models, even when the initial stress field is quite homogeneous. We also find that the interaction between fault geometry and stress pattern helps to explain other observations in this event, including slow rupture propagation on the northwest branch. The results help to show that 3D dynamic effects may be crucial in determining rupture propagation and slip behavior on geometrically complex fault systems, although these effects may be hard to predict without detailed knowledge of the stress pattern and fault geometry prior to earthquakes.

Introduction

Studies of recent earthquakes have made it increasingly clear that earthquake faults are generally not simple planar features. The 1992 Landers, California (Sieh *et al.*, 1993), 1999 Izmit, Turkey (Toksoz *et al.*, 1999), and 1999 Hector Mine, California (Scientists from the USGS *et al.*, 2000), events have emphasized that strike-slip earthquakes commonly take place on faults that display multiple offset fault segments with gaps and different orientations. The **M** 7.1 Hector Mine event in particular ruptured a north–south–trending fault system, with a complicated branching structure in both its northern and southern ends (Fig. 1).

This structure has been identified by field mapping (Scientists from the USGS *et al.*, 2000), aftershock studies (Hauksson *et al.*, 2002), strong motion and static deformation models (Ji *et al.*, 2002; Kaverina *et al.*, 2002; Simons *et al.*, 2002), and trapped wave studies (Li *et al.*, 2002a,b). These studies suggest that the hypocenter was located on the most northeastern segment, approximately 4 km north of the northern bifurcation point, although nucleation either directly on the segment junction or just to its south cannot be categorically ruled out. Strong motion models (Ji *et al.*, 2002; Kaverina *et al.*, 2002) indicate that the two northern segments experienced roughly similar amounts of moment release. In spite of this similarity, there was a qualitative difference between the slip patterns on the two northern branches: direct observations (i.e., field mapping) (Scientists from the USGS *et al.*, 2000) indicate that the northwest branch on the Lavic Lake fault (LLF) ruptured up to the surface, while the north branch did not. However, the aftershock studies, strong motion studies, and trapped wave studies cited earlier imply that the north branch experienced significant slip at depth in this event and that this slip extended close to the surface. Taking these observations and modeling results at face value, Li *et al.* (2002b) have argued (using simple dynamic models) that this feature of the slip pattern on the northern branch caused the rupture to propagate to the northwest branch, in spite of the fact that slip on the north branch should have caused most of the north branch to be in a stress shadow. The present article verifies this claim through more accurate and realistic dynamic models, and it also explores in detail some of the issues involved in inducing slip on fault segments that appear to be unfavorable for rupture.

Much work has been devoted in recent years to accurate

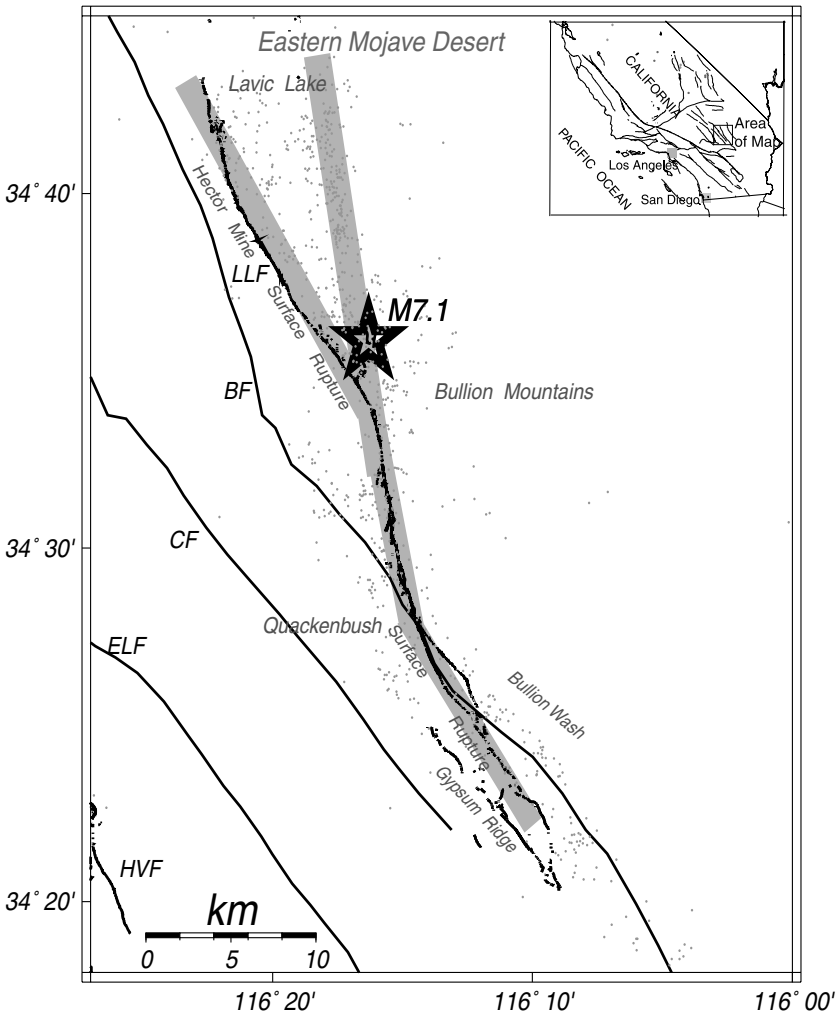

Figure 1. Map of the 1999 *M* 7.1 Hector Mine earthquake, including mapped surface rupture (rough dark lines), mapped nearby faults (smooth dark lines), inferred branched fault geometry (thick gray lines), epicenter (star), and aftershocks (dots). After Li *et al.* (2002b) and Scientists from the USGS *et al.* (2000).

dynamic models of faults with nontrivial geometry. The goals have included a better understanding of the processes by which earthquakes can propagate around corners and across segment boundaries, increasing the size of the final event. The initial work in this area was performed by Harris *et al.* (1991) and Harris and Day (1993) on parallel fault segments. They used 2D dynamic models to explore how fault offset distance, overlap direction, and overlap amount affect the ability of earthquakes to jump across segment boundaries. This work was extended to faults with bends (Bouchon and Streiff, 1997), orthogonal fault segments with offsets (Kase and Kuge, 1998), extended to 3D (Harris and Day, 1999; Kase and Kuge, 2001), and to 3D segments with offsets and branches (Aochi *et al.*, 2000, 2002). Aochi and Fukuyama (2002) applied the methodology of Aochi *et al.* (2000) to model the effect of complex fault geometry on the 1992 Landers earthquake. They found that the areas with strike changes appeared to correspond with regions of small slip in both the model and the actual fault. Harris *et al.* (2002) modeled the dynamics of the 1999 Izmit, Turkey, earthquake and found that even a 20° change in strike between segments did not serve as a barrier to rupture propagation. Poliakov *et al.* (2002) examined in detail the conditions under which ruptures will propagate to off-axis branching faults. They determined that off-axis branching depended strongly on both the ambient stress field as well as the speed of rupture propagation and the mode of fracture. Kame *et al.* (2003) extended this work to address the persistence of rupture on different fault branches. They found that the dynamic stress interaction between the branches could determine the ability of rupture to continue or die out on each branch. Oglesby *et al.* (2003) modeled the dynamics of two overlapping thrust faults. They found that the ability of the rupture to jump from one segment to another was related to the degree of overlap and that stress heterogeneity could greatly aid the ability of rupture to make this jump. The former point is of direct importance to the current work on the Hector Mine event.

As mentioned before, much of the present work is focused on exploring (through 3D dynamic models) how the Hector Mine earthquake could have propagated to the northwest (LLF) segment as well as the northern segment. This article continues the preliminary work by Li *et al.* (2002b) by (1) introducing a more accurate fault geometry, (2) in-

cluding the effects of different shear and normal stresses due to their different orientations with respect to the tectonic stress field, (3) experimenting with different hypocenter locations and different stress distributions to explore the sensitivity of the results, and (4) using a time-dependent coulomb stress analysis to gain insight into the conditions under which rupture is favored to propagate to the northwest branch. We find that the main prediction of Li *et al.* (2002b) is validated: the fact that slip on the northern branch did not propagate to the surface causes the near-surface region of the northwest branch to be brought closer to failure, allowing the earthquake to rupture both branches instead of just the north branch. We also find that the results are highly insensitive to details of hypocentral location and stress pattern. An additional result is that it may be much more difficult for ruptures to jump segment boundaries at depth than near the surface.

Methods

We use the 3D explicit finite-element method (Whirley and Engelmann, 1993; Oglesby, 1999) for our dynamic faulting models. Faults are modeled as planes of split nodes with zero width. Forces and displacements are calculated directly on these split nodes, and the fault segments can have arbitrary orientation in space. Our fault constitutive law utilizes a coulomb friction law for the shear stress τ and a linear slip-weakening relationship (Ida, 1972; Andrews, 1976) for the coefficient of friction μ:

$$|\tau| \leq -\mu\sigma_n, \tag{1}$$

where

$$\begin{aligned} \mu &= \mu_{\text{static}} - (\mu_{\text{static}} - \mu_{\text{sliding}}) \left(\frac{s}{d_0}\right) (s \leq d_0), \\ \mu &= \mu_{\text{sliding}} \ (s > d_0), \end{aligned} \tag{2}$$

s is the magnitude of the slip (displacement discontinuity) vector across the fault, τ is the shear stress across the fault, σ_n is the effective (total normal stress minus pore fluid pressure) normal stress across the fault (negative in compression), and d_0 is the critical slip-weakening distance. Since s, τ, and σ_n can vary with time, this relatively simple friction law can lead to quite complicated dynamic behavior when fault geometry is complex.

The modeled fault geometry is shown in Figure 2a, and the corresponding finite-element mesh is shown in Figure 2b. For simplicity, the fault segments are all vertical, and the material is a homogeneous half-space. We use a simple material structure in order to isolate the aspects of the Hector Mine event that are attributable to fault geometry alone. More accurate models with inhomogeneous material structure are being developed as part of the larger research project of this group. The finite-element model region is embedded

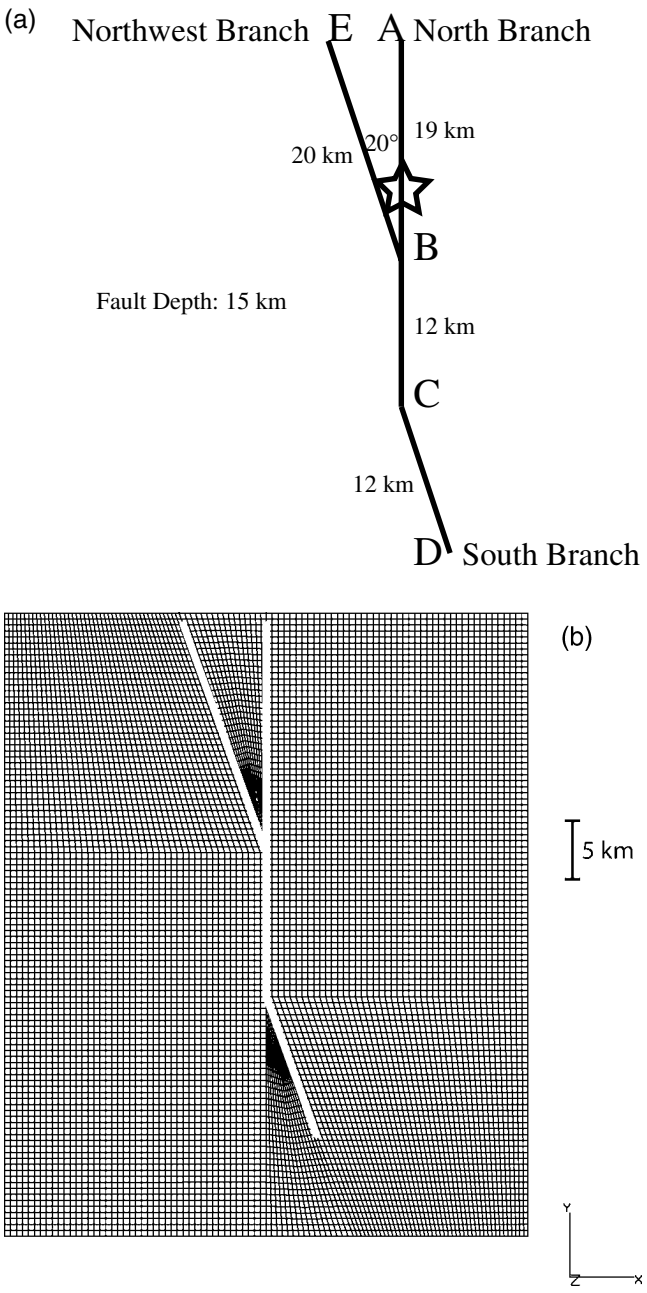

Figure 2. Fault geometry used in the dynamic models. (a) Map view of fault geometry. Segment names are identified, with the preferred hypocenter marked with a star. The letters denote a set of reference points along the fault system. (b) Map view of finite-element mesh used in dynamic models. Fault segments are shown in white.

in a much larger buffer region (roughly 60 km in radius) to eliminate artificial reflections from the edges of the finite-element mesh. In our preferred model, nucleation takes place 4 km north of the northern segment junction, at a depth of 7.5 km. Nucleation is accomplished by bringing nodes to their failure stress inside a nucleation zone of radius 3 km. Inside this zone, the rupture is forced to propagate at a speed

of 3.0 km/sec. Outside this zone, the rupture propagates spontaneously. The material and computational parameters are given in Table 1. The assumed parameters lead to a maximum resolved frequency of approximately 0.6 Hz.

Our choice of stress field requires detailed explanation. Except where noted in the text, our stress does not change with depth. Since the normal stress in our models takes the pore pressure into account, our depth-independent normal stress can be thought of as being due to pore pressure that increases at such a rate as to cancel out the increase in the absolute level of normal stress—clearly an approximation, but one that results in the desired effect that the stress drop does not vary significantly with depth. Other ways to achieve this goal exist include using a depth-dependent frictional coefficient (Aagaard *et al.*, 2001). As will be noted in the Discussion, models in which the stress drop tapers to zero in the near-surface region produce results very similar to those of our constant-stress-drop models. Our values for shear and normal stresses on the main fault strike (connecting the northern segment to the southern segment in Fig. 2) are consistent with a tectonic stress field with the principal compressive stress oriented roughly 30° east of north, a stress orientation similar to that of Hauksson *et al.* (2002). For an isolated fault with our choice of static and dynamic frictional coefficients (0.7 and 0.5, respectively), these stresses lead to a stress drop of 30 bars. Such a choice leads, as we shall see, to a modeled seismic moment quite comparable to that observed in the actual event, and it is consistent with the 25-bar estimate of Ji *et al.* (2002). In Li *et al.* (2002b), we simply assigned the same shear and normal stresses to all fault segments, to isolate the purely dynamic effects of the changes in strike. In the present work, we rotate the tectonic stress field to the segments of different orientation. However, to simply do so results in shear and normal stresses that are highly unfavorable to rupture on the northwest and southern fault segments. Thus, the observed rupture pattern requires either additional shear stress or a reduction in normal stress amplitude to be assigned to these segments. We choose the former method, leading to an effective rotation of the tectonic stress field in these parts of the fault. This method is somewhat similar to that of Aochi and Fukuyama (2002), who needed to slightly rotate the tectonic stress field along the Landers fault to allow the rupture to propagate along the observed fault geometry (consistent with the low strength excess in the northwest part of the Landers fault system discussed by Bouchon *et al.* [1998]). A plausible explanation for the additional shear stress needed on these segments is that each segment has a different rupture history. The stress field on each segment is due to both the ambient tectonic stress field and all the earthquakes that have taken place on or near that segment. The northwest and southern segments may be less favored for rupture by virtue of their orientation, but may have experienced a longer interseismic loading time than the northern segment. Thus, they can build up greater shear stress, leaving them favorable for rupture in the Hector Mine event. While the observed fault geometry seems to demand such a stress field, we will show in the Results that the effects we investigate are rather insensitive to the assumptions we make about the stress field on the different segments, as long as the segments are reasonably close to failure.

An additional aspect of the modeled stress field is that in some simulations, we assign stress in such a way as to prevent the rupture from propagating to the surface or to great depth. In the former case, the reason for this assignment is to match the observation that there was no slip on this part of the fault (Scientists from the USGS *et al.*, 2000). We simply treat this observation as a boundary condition and choose a method to impose it on our model. One method of accomplishing this task would be to assign a high-amplitude clamping normal stress to the fault in the nonslipping areas. However, it is hard to justify very high normal stress amplitude so close to the surface. Thus, our preferred method is to reduce the initial shear stress to zero in the areas that we do not want to rupture. Thus, rupture has no elastic energy to release and dies out shortly after entering these zones (Archuleta and Frazier, 1978; Day, 1982). While an investigation into the physical reason for this low shear stress is not part of this work, one physical hypothesis to justify this assignment would be that this portion of the fault slipped

Table 1
Material and Computational Parameters

Density	2800 kg/m^3
V_P	6300 m/sec
V_S	3600 m/sec
Initial shear stress (north segment)	130 bars
Initial shear stress (northwest and south segments)	177 bars
Initial normal stress (north segment)	−200 bars
Initial normal stress (northwest and south segments)	−287 bars
Static frictional coefficient	0.7
Sliding frictional coefficient	0.5
Fault element size (north segment)	500 m × 500 m
Fault element size (northwest and south segments)	532 m × 500 m
d_0	0.4 m
Maximum frequency	~0.6 Hz

in a recent, smaller event and has not had enough time to accumulate shear stress. Alternatively, this zone could be very weak and unable to withstand enough of a stress buildup to allow unstable slip. For the models that have no slip over a defined region at depth, we simply increase the normal stress amplitude over this region to pin the fault there. Tests have shown that the results are quite insensitive to the specific assumption we make as to how rupture is stopped: as long as rupture does not propagate to the free surface on the north branch for some reason, the rupture and slip patterns on the rest of the fault system are quite robust.

In addition to our dynamic analysis, we also perform a time-dependent stress transfer analysis to gain further insight into the nature of stress interaction between the fault segments. This analysis begins by running a dynamic rupture model on the north and south segments in the absence of the northwest segment. This model produces as its output, in addition to the slip on the ruptured faults, the time-dependent stress distribution on the plane of the northwest segment. We can use this stress distribution to calculate the time-dependent coulomb failure stress increment [$\Delta\text{CFS} = \Delta\tau + \mu(\Delta\sigma_n)$] on this plane to determine when and where it has been brought closer to or farther from failure. While these simulations are somewhat artificial, they allow us to study the effect that the north branch has on the northwest branch, without the complication of the effect of slip on the northwest branch.

Results

Prior to presenting our preferred dynamic model for the Hector Mine earthquake, we first show a detailed analysis of the (artificial) case in which rupture is allowed to proceed all the way to the free surface on the north segment. Then, we present our preferred model of this event, in which rupture dies out 1 km from the surface on the northern segment. We also present variations on the model to show the sensitivity of the results with respect to the prestress pattern on the fault segments and the hypocenter location.

Rupture Allowed to Propagate to Surface on North Segment

In this model no constraints are placed on the stress field to cause rupture to die out near the surface of the north segment. Snapshots of the development of slip in this system are shown in Figure 3. The rupture is nucleated at $t = 0$ sec. At $t = 2.0$ sec, rupture has nucleated on the north branch and is about to reach the intersection with the northwest branch at 20 km along strike (note that the branch's northern edge is at roughly 1 km along strike according to this coordinate system). At $t = 6.7$ sec, the rupture has proceeded over the entire north segment and has started to propagate around the change in strike to the south segment. At the end of the simulation ($t = 19.9$ sec), the north and south branches have completely ruptured, but the northwest branch has experienced no slip.

Snapshots of shear and normal stress (Fig. 4) help to explain why, in this case, rupture does not propagate to the northwest segment. At $t = 2.0$ sec, we see a typical elliptical rupture front on the north branch, and we see that a complicated pattern of shear and normal stress is transferred to the northwest branch. Approximately speaking, in the part of the northwest branch that overlaps with the slipping (or slipped) region of the north branch, both shear and normal stress amplitudes are reduced. Even though the increments in normal and shear stress work in opposite directions (reducing shear stress sends the segment farther from rupture, while decreasing normal stress amplitude brings the segment closer to failure), the net effect in this region is to send the northwest branch farther from rupture. Conversely, in the parts of the northwest branch that overlap the unruptured part of the north branch, shear and normal stress amplitude are increased, and the segment is brought closer to failure.

At $t = 5.0$ sec, the rupture front has propagated over almost the entire north branch, and the northwest branch experiences a somewhat more complicated stress pattern than described earlier (since the interacting regions of the north and northwest branches are much closer in the earlier snapshot, due to the rupture front being close to the segment intersection). However, there is still no part of the northwest branch that is brought to failure by slip on the north branch. Finally, at $t = 19.9$ sec, rupture has proceeded over the entire north and south branches.

Rupture Constrained to Stop 1 km from Surface on North Segment

As argued by Li *et al.* (2002b), constraining the rupture not to reach the free surface on the north branch (north of the segment intersection) can cause part of the northwest branch to be brought to failure, leading to rupture on both branches. Our current results use different fault geometry and stress distributions, but we find that the main result of Li *et al.* (2002b) remains. The snapshots of slip propagation shown in Figure 5 initially look very much like those for the case in which rupture was allowed to the free surface on the north branch (Fig. 3). However, at $t = 6.7$ sec, rupture has propagated over much of the north branch, creating a large stress concentration at the upper-right corner of the northwest branch. At this time, slip has already nucleated at the predicted location and is starting to propagate over the northwest branch. At $t = 19.9$ sec, this slip has propagated over the entire north branch. Thus, the model that is designed not to produce slip at the surface of the north branch automatically produces slip on the northwest branch, in agreement with observations. Another important feature of the dynamic model is that there is a large discontinuity in the slip between the parts of the north segment on either side of the intersection with the northwest branch at 20 km along strike. This discontinuity is due to the slip on the central part of the fault being affected by slip on both the north and northwest branches, a two-way stress interaction that requires a full dynamic model to capture.

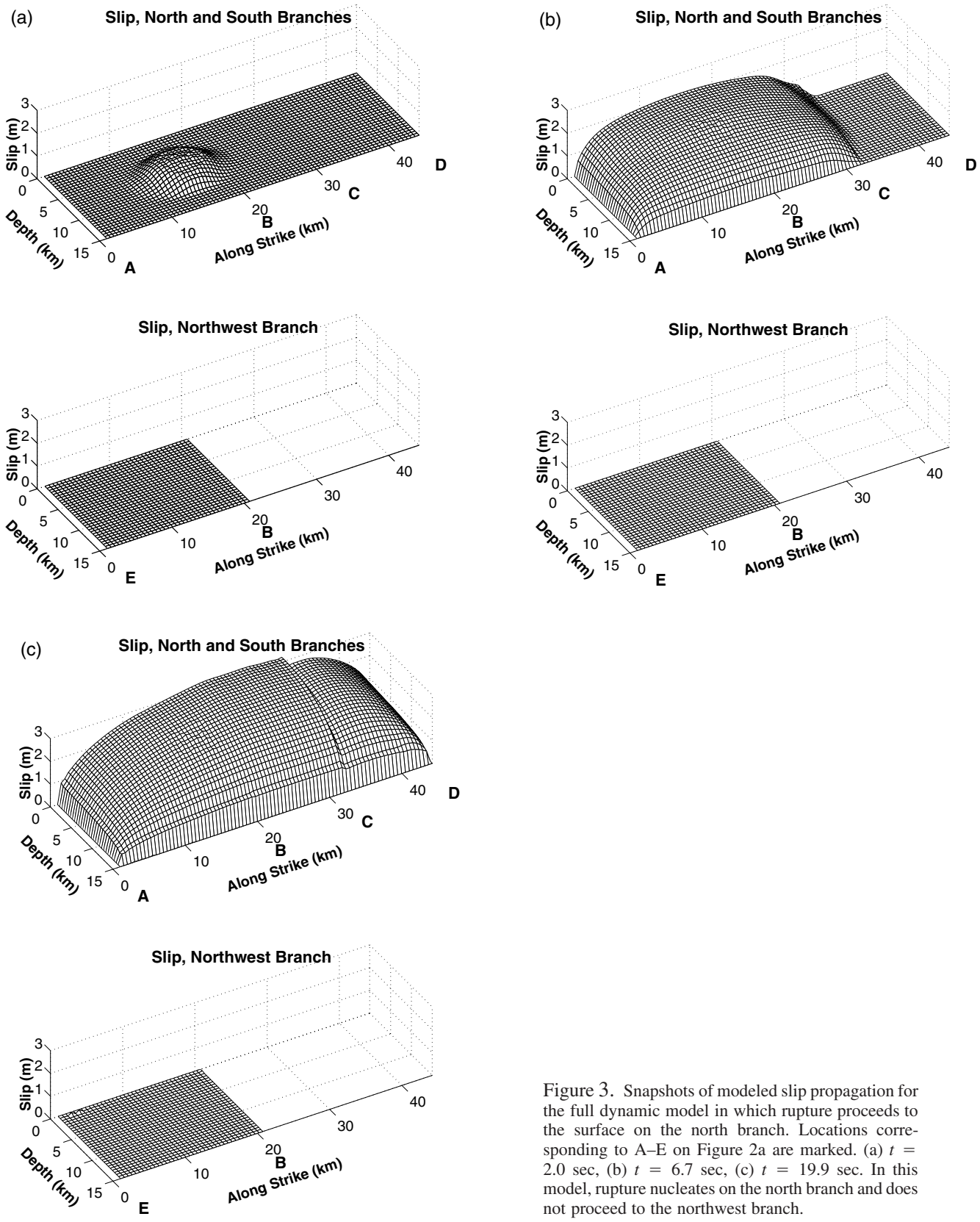

Figure 3. Snapshots of modeled slip propagation for the full dynamic model in which rupture proceeds to the surface on the north branch. Locations corresponding to A–E on Figure 2a are marked. (a) t = 2.0 sec, (b) t = 6.7 sec, (c) t = 19.9 sec. In this model, rupture nucleates on the north branch and does not proceed to the northwest branch.

The difference between this model and the model in which rupture is allowed to the free surface on the north branch is clarified by snapshots of stress in Figure 6. As in the previous model, the rupture front on the north branch displays a typical elliptic shape at $t = 2.0$ sec. Shear and normal stress are modified on the northwest branch, but not enough to bring the northwest branch above its failure threshold. By $t = 5.0$ sec, the rupture front has propagated to the free surface on the southern part of the north branch and has died out near the free surface on the majority of the north branch. The heterogeneous slip pattern on the north branch has induced a much more complicated stress pattern on the northwest branch, with shear and normal stress amplitudes largely reduced on the part of the northwest branch overlapping the slipping (or slipped) region of the north branch, but with the opposite pattern on the near-surface part of the northwest branch, which overlaps the unslipped region of the north branch. While increases in both shear and normal stress amplitudes work in opposite directions in bringing the segment closer to rupture, the net effect is to bring the northwest segment closer to failure. At $t = 5.2$ sec, the top right corner of the northwest branch fails, and a rupture front starts to propagate across this branch. This secondary rupture front is visible in the snapshot at $t = 11.5$ sec. Finally, after rupture has proceeded across the three fault branches ($t = 19.9$ sec), the system is left in a much more heterogeneous state of stress than that in which it started, with large build-ups and reductions of shear and normal stress amplitude on either side of the segment boundaries.

Additional insight into the reasons behind rupture propagation to the northwest branch can be gained by examining the time-dependent change in the coulomb failure stress (ΔCFS) on the northwest segment. As mentioned in the Methods, for this analysis we do not allow slip on the northwest segment and simply follow the time-dependent (dynamic) stress field on the northwest segment induced by the north and south segments. The distribution of ΔCFS on the northwest fault branch is shown in Figure 7. At $t = 2.0$ sec, the slipping region of the north segment has brought a large area of the northwest segment farther from failure, corresponding to negative ΔCFS. However, by $t = 5.2$ sec, the slip gap at the surface of the north segment has caused the region of the northwest branch near the surface to be brought closer to failure, with a small region (near the branch intersection) brought above the failure criterion of $\Delta\text{CFS} = \Delta\tau + \mu(\Delta\sigma_n) = 24.0$ bars. Finally, at $t = 20.0$ sec, the area of the northwest segment brought above the failure stress grows, while most of the segment is below the failure limit. The two northern fault segments are nearly parallel and very close, so a simple way to interpret this analysis is to note that the northwest branch is sent farther from failure in areas where it overlaps the slipped region of the north branch and is brought closer to failure in areas where it overlaps the unslipped region of the north branch. The large induced positive ΔCFS is amplified by the edge of the slipping region on the north branch near the surface at roughly 20 km along strike, where there is a corner in the slip distribution as the slip transitions from buried to surface reaching. Great slip heterogeneity, coupled with large slip amplitude, leads to large stress increments off the fault plane. It should be noted that the final stress pattern ($t = 20.0$ sec) corresponds to a static stress analysis for rupture on the north and south branches. Thus, in this case even a static analysis predicts that rupture on the north and south branch should bring at least a portion of the northwest branch to failure and lead to propagating rupture on this branch. A similar analysis for the case in which slip is allowed to propagate to the surface of the north segment shows that no part of the northwest branch is brought above its coulomb failure stress level, further explaining the contrasting behaviors in the two models.

Experiments with Different Stress Distributions and Hypocenters

While the preferred model for the Hector Mine event reproduces general features of the observed slip pattern (in particular, the propagation of rupture to the northwest branch, with similar moments on both northern branches), it is important to determine how finely tuned a model must be to give similar results. Toward this goal, we have experimented with numerous additional models that do not necessarily match the observed earthquake as well, but serve to illustrate the sensitivity of the results to assumptions about the stress field and hypocenter location.

Same Shear and Normal Stress on All Segments. In this model, we assign the same shear and normal stresses (equal to the stresses on the north branch in the preferred model) to all fault branches. This model is similar to that of Li *et al.* (2002b), except in this case rupture is allowed to progress up to 1 km from the surface of the Earth, rather than 5 km as in Li *et al.* (2002b). Figure 8 displays the resultant slip pattern, which is quite similar to that of the preferred model (final frame of Fig. 5). The only difference is that with a slightly smaller initial stress on the northwest and south segments, there is a slightly smaller stress drop and slightly smaller slip.

Rupture Constrained to Stop 5 km from Surface on North Segment. This model is also somewhat similar to that of Li *et al.* (2002b), except that we use the shear and normal stresses of our preferred model. The smaller slipping region on the north segment leads to greatly reduced slip on this segment (Fig. 9), but in this case rupture still proceeds to the northwest segment, leading to general agreement with the observed surface slip. However, the match to slip inversions such as that of Kaverina *et al.* (2002) is not as good as with the preferred model, which had much more similar moment release between the two northern segments.

Rupture Constrained to Stop 5 km from Base of North Segment. An important question raised by the preferred model concerns the role of the free surface in facilitating

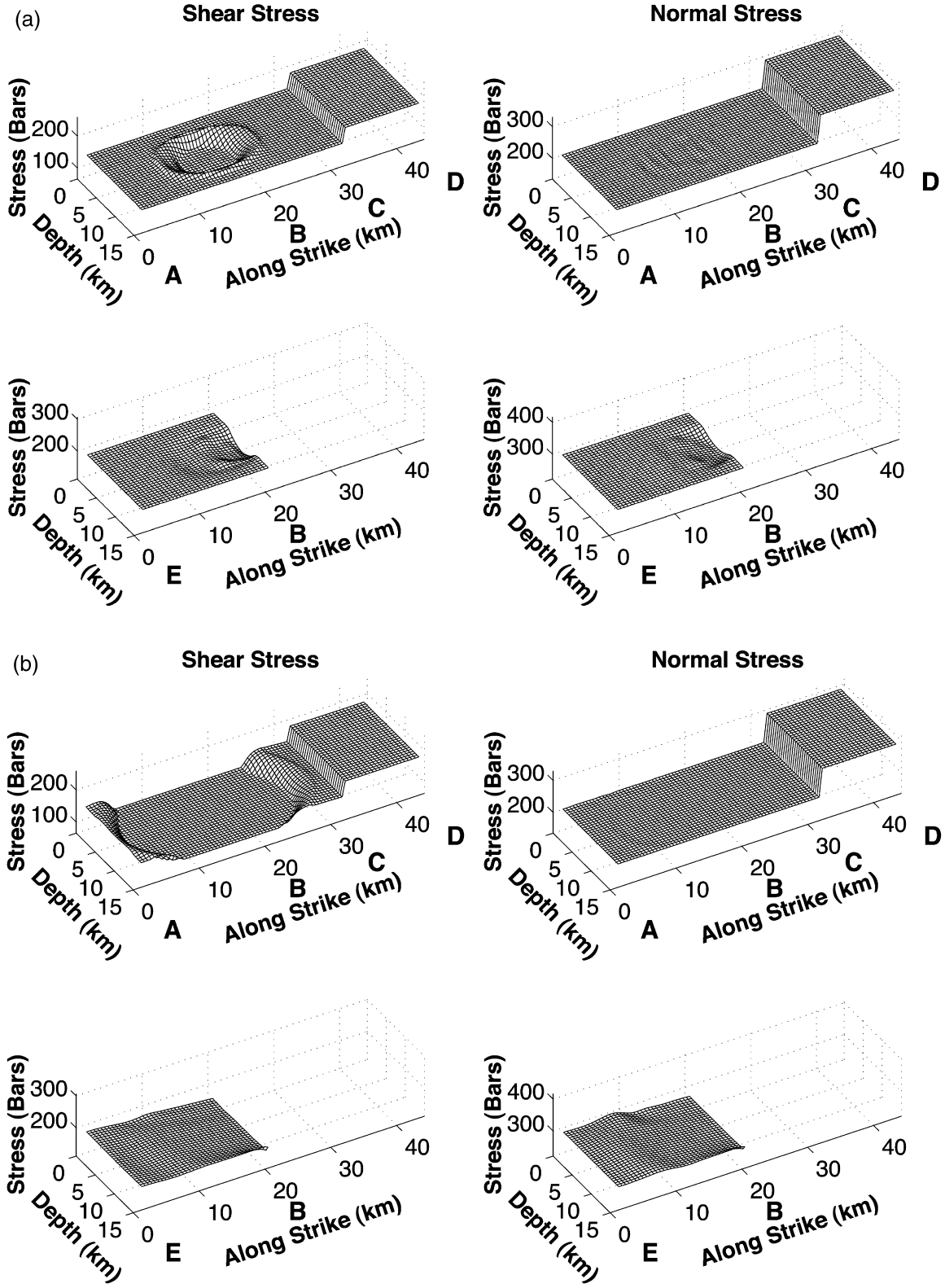

rupture progression from the north to the northwest segment. To test the effect of the free surface, we constructed models in which the rupture was permitted to propagate all the way to the surface of the north segment, but was constrained not to proceed to the base of that segment. This constraint should result in a positive ΔCFS at the base of the northwest segment (rather than at the surface) and possibly lead to jumping rupture at this point. These models are somewhat artificial, in that they do not reproduce the observed surface slip pattern. Experiments with rupture constrained to stop 1 and

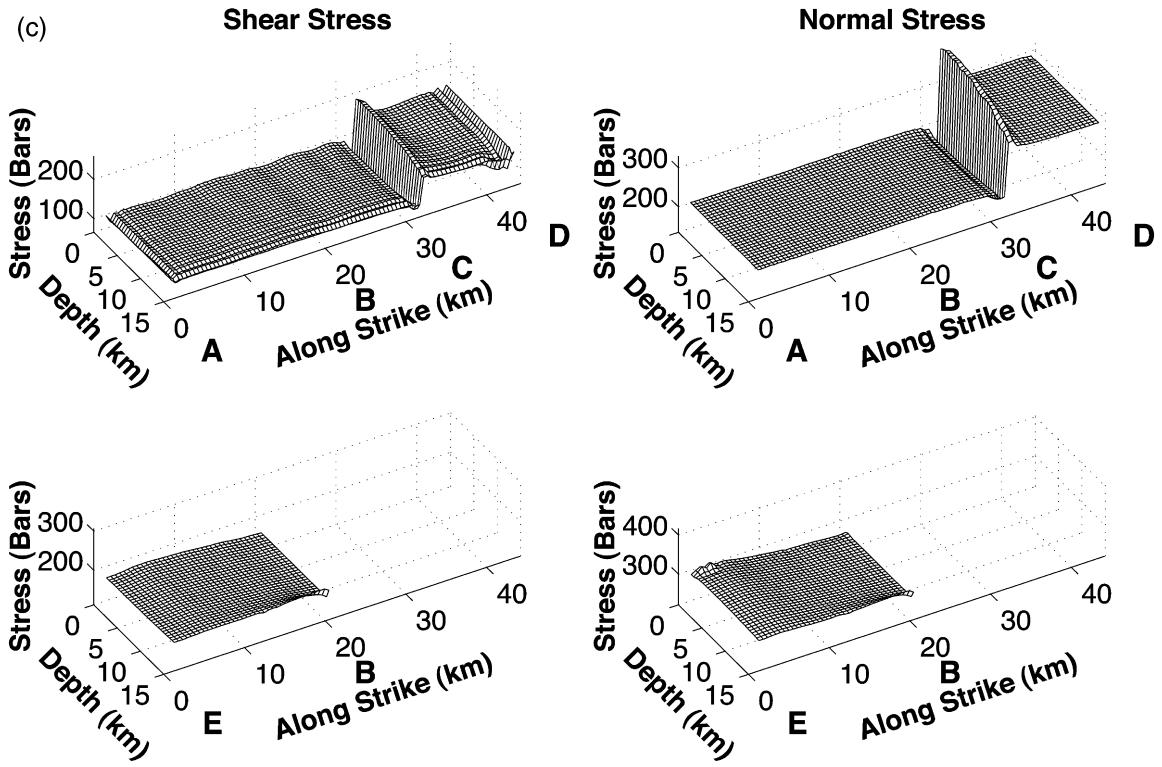

Figure 4. Snapshots of modeled stress on the fault for the full dynamic model in which rupture proceeds to the surface on the north branch. Locations corresponding to A–E on Figure 2a are marked. Shear stress is displayed on the left panels, and normal stress is displayed on the right. The north and south branches are displayed on the top panels, and the northwest branch is displayed on the bottom. (a) $t = 2.0$ sec, (b) $t = 5.0$ sec, (c) $t = 19.9$ sec. In this model, rupture nucleates on the north branch, and does not proceed to the northwest branch.

3 km from the base of the north segment produced either no transfer of rupture to the northwest segment (in the former case) or a delay of over 10 sec before rupture propagation onto the northwest segment (in the latter case). Only when rupture was halted 5 km from the base of the north segment did the rupture proceed with similar timing (delay of approximately 6.9 sec) onto the northwest segment. The slip distribution resulting from this model is shown in Figure 10. The requirement for a greater area with zero slip on the north segment (compared with the preferred model) in this case shows that the free surface greatly facilitates the propagation of rupture to the north segment. This issue will be explored in detail in the Discussion.

Rupture Nucleates on the Stem, South of the Segment Junction. While the studies cited in the Introduction have argued that the hypocenter of the Hector Mine event is on the north segment, north of the segment junction, a location on either the stem (south of the segment junction), the junction, or the northwest segment cannot be categorically ruled out. Therefore, we have carried out calculations with the same stress distribution as in our preferred model, but with the hypocenter located in these alternative positions. When the hypocenter is on the stem, we find results that are almost identical to the preferred model, as is illustrated in Figure 11. Not only is the slip distribution very similar to our preferred model (Fig. 5), but also the timing of the rupture propagation on the northwest segment is very similar (with rupture beginning on this segment 4.5 sec after nucleation on the main fault segment). When we allow rupture to proceed all the way to the free surface on the north segment with the hypocenter on the stem, rupture does not proceed to the northwest segment. Thus, our results are essentially the same whether the earthquake nucleates on the stem or on the north branch. Because of their similarity, it may be hard to differentiate between these two models, at least at the low frequencies in this current dynamic study. Of course, directivity in the ground motion will be slightly different between these two models, so strong motion inversions may be able to differentiate between these two cases (although no such differentiation has been unequivocally shown to date).

Rupture Nucleates on the Segment Juction. The model of Kaverina *et al.* (2002) places the hypocenter directly at the junction between the northwest and north branches. Our dynamic model with nucleation at this junction produces a slip pattern nearly identical to both our preferred model and the stem-nucleation model given earlier. Rupture timing is quite

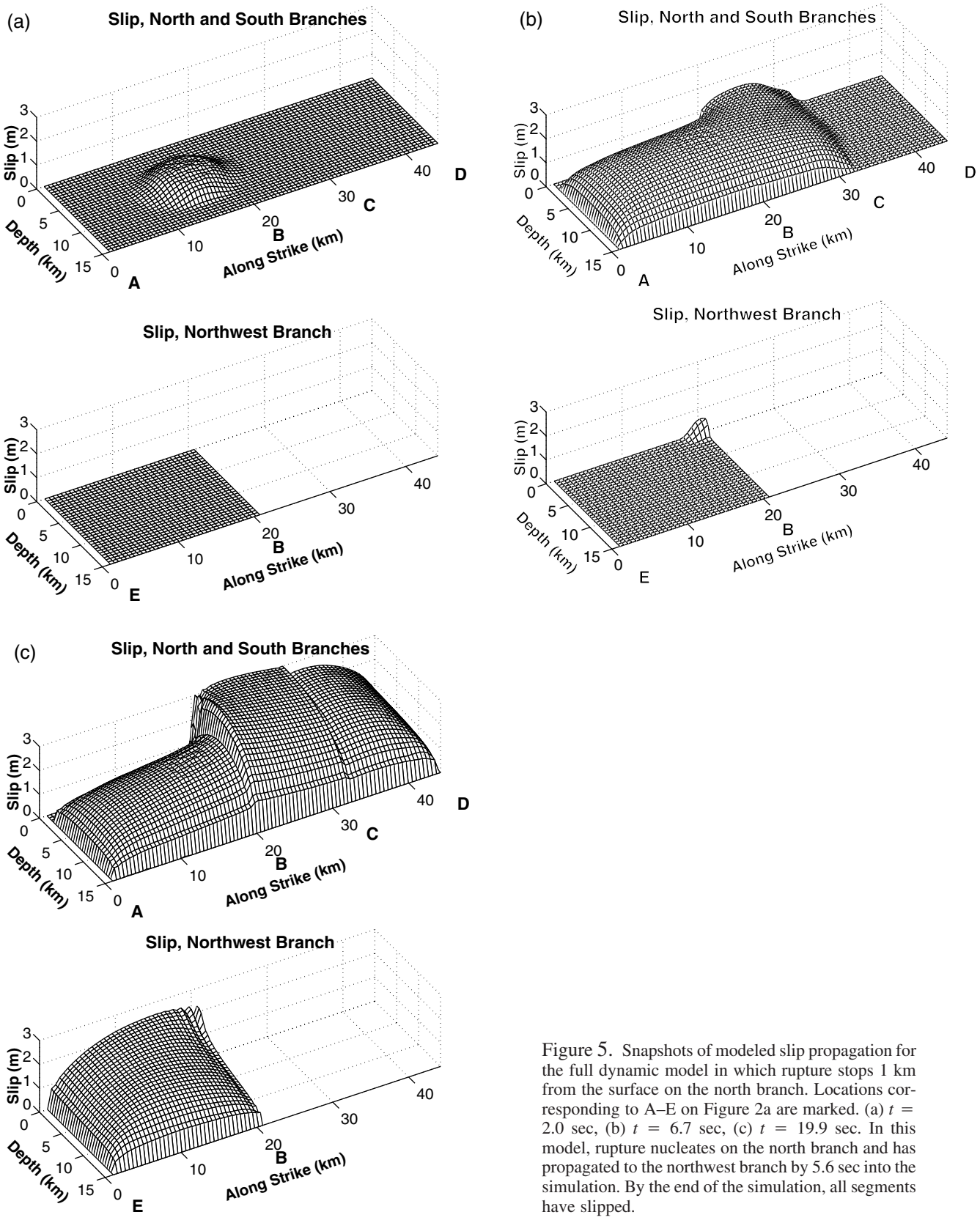

Figure 5. Snapshots of modeled slip propagation for the full dynamic model in which rupture stops 1 km from the surface on the north branch. Locations corresponding to A–E on Figure 2a are marked. (a) t = 2.0 sec, (b) t = 6.7 sec, (c) t = 19.9 sec. In this model, rupture nucleates on the north branch and has propagated to the northwest branch by 5.6 sec into the simulation. By the end of the simulation, all segments have slipped.

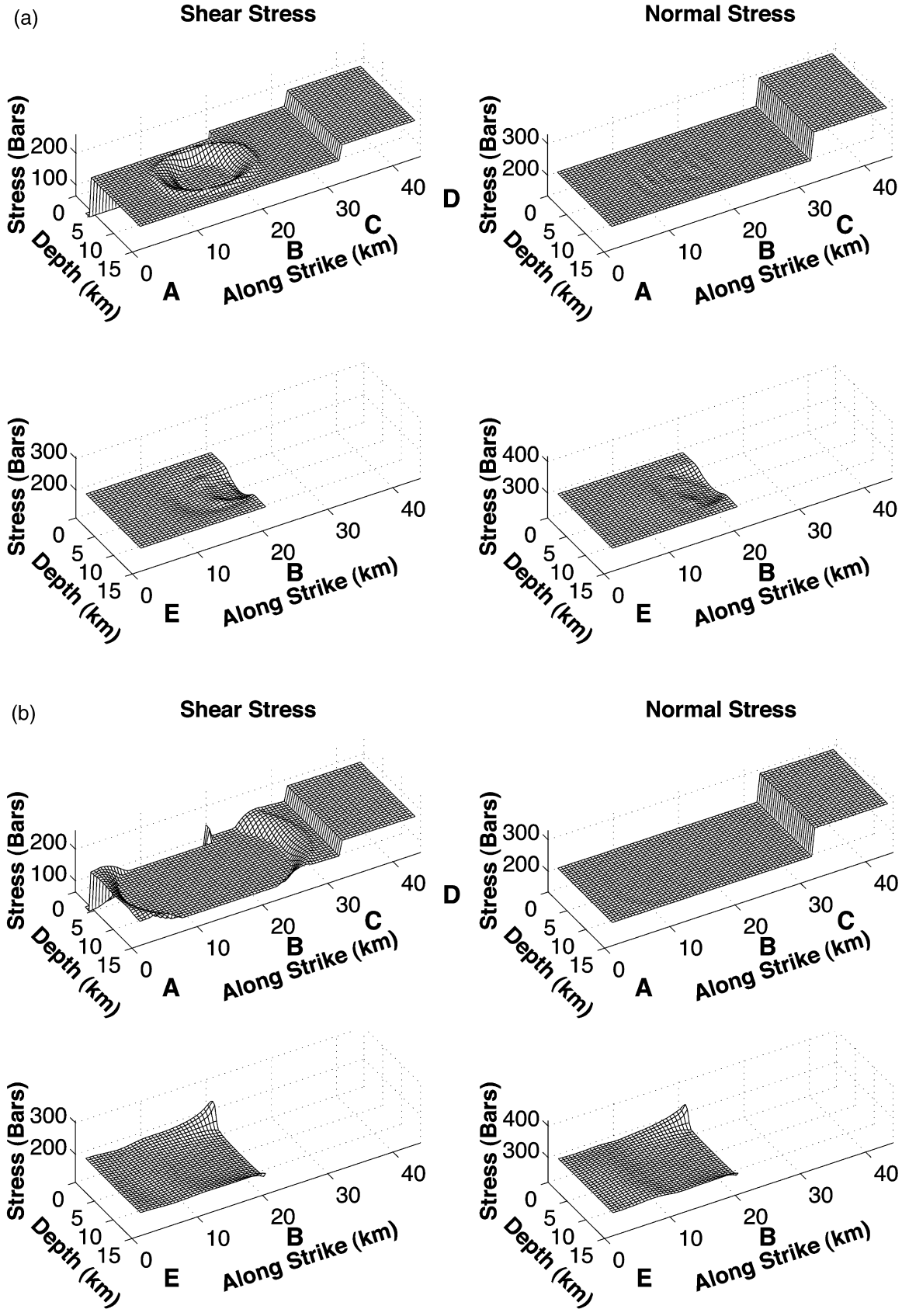

Figure 6. Caption on next page.

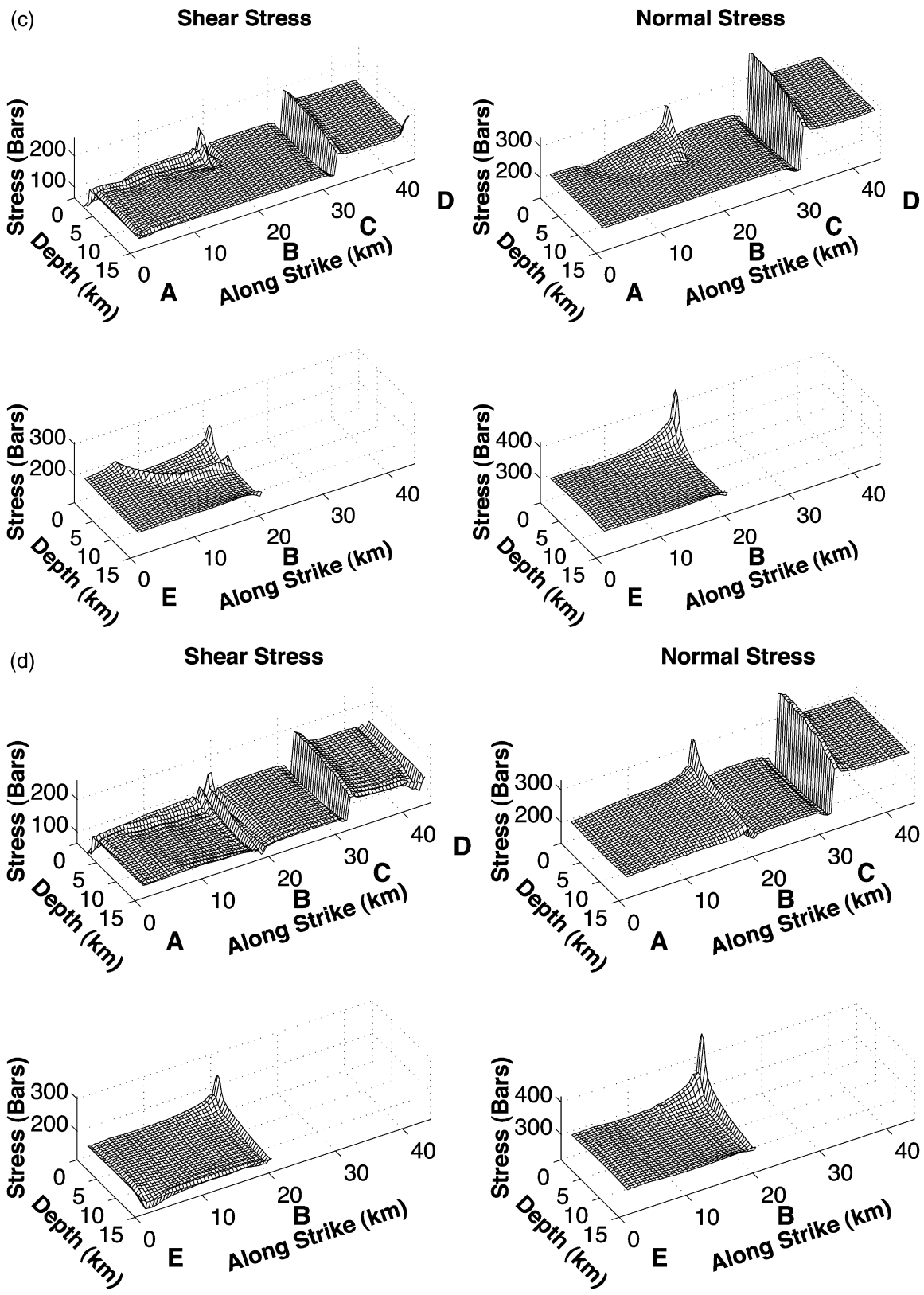

Figure 6. Snapshots of modeled stress on the fault for the full dynamic model in which rupture stops 1 km below the surface on the north branch. Locations corresponding to A–E on Figure 2a are marked. Shear stress is displayed on the left panels, and normal stress is displayed on the right. The north and south branches are displayed on the top panels, and the northwest branch is displayed on the bottom. (a) $t = 2.0$ sec, (b) $t = 5.0$ sec, (c) $t = 11.5$ sec, (d) $t = 19.9$ sec. In this model, rupture nucleates on the north branch and has propagated to the northwest branch by 5.2 sec into the simulation. By the end of the simulation, all segments have slipped. Note the highly heterogeneous final stress pattern, compared to the relatively homogeneous initial stress pattern.

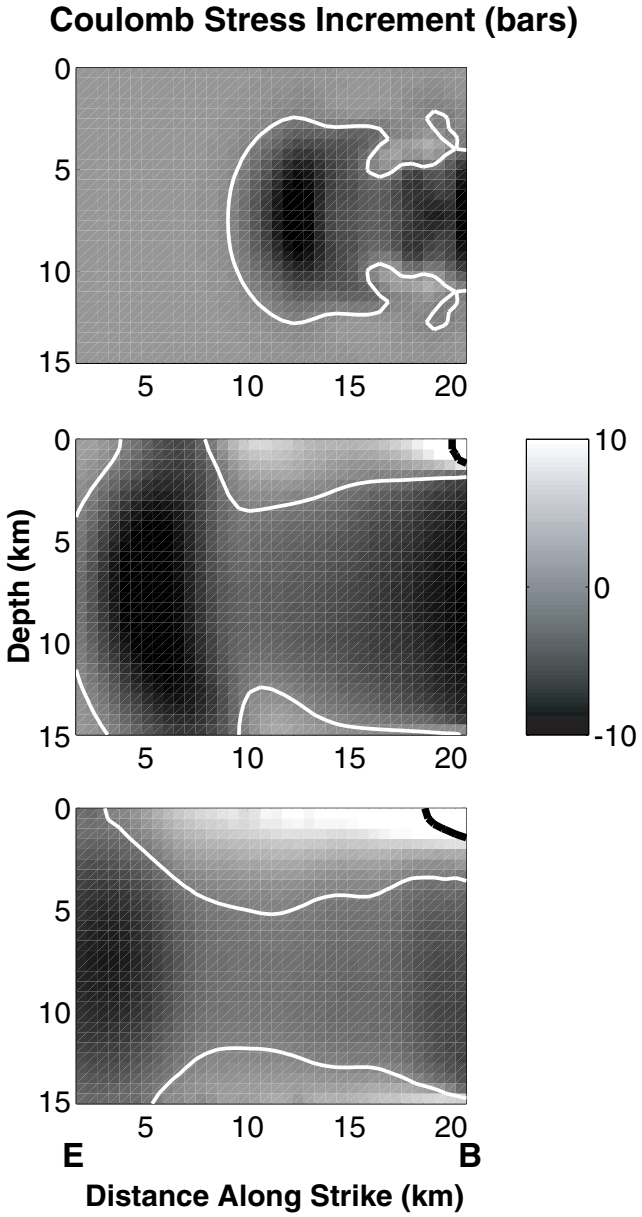

Figure 7. Snapshots of modeled time-dependent coulomb failure stress on the plane of the northwest segment due to slip on the north and south segments. In this case, rupture is constrained not to reach the surface of the north branch. Top frame, $t = 2.0$ sec; middle frame, $t = 5.2$ sec; bottom frame, $t = 20.0$ sec. The white contour marks zero change in ΔCFS, while the black contour marks the failure threshold of ΔCFS = 24.0 bars. The upper part of the northwest segment closest to the branch point is brought above its failure stress by slip on the north branch.

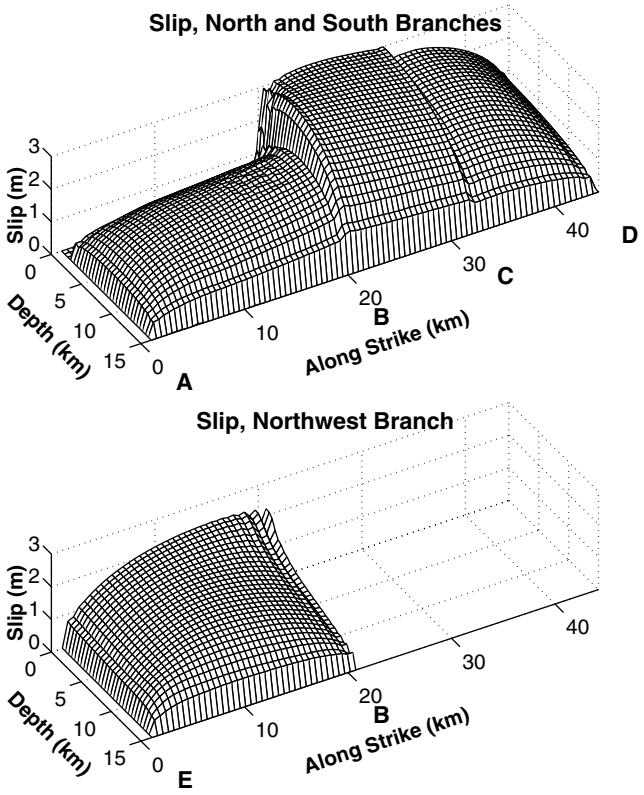

Figure 8. Final modeled slip distribution for the model in which shear and normal stresses are the same on all fault segments. Locations corresponding to A–E on Figure 2a are marked. The slip distribution is quite similar to that of the preferred model (Fig. 7c).

similar to the stem-nucleation model, with rupture beginning on the northwest segment 4.6 sec after overall nucleation.

Rupture Nucleates on the Northwest Segment. When we nucleate rupture on the northwest segment, the north segment falls largely into the stress shadow of the northwest segment. This model produces the final slip pattern shown in Figure 12. The small amount of slip on the northern part of the north branch occurs when slip reaches the northern edge of the northwest branch, bringing a small part of the north branch to failure. However, this slip is very small and dies out well north of the segment boundary. Thus, it appears that while a hypocenter on the northwest branch cannot be ruled out, it would require different (and likely more complicated) assumptions about the stress field than we make in our model and is considerably less likely.

Discussion

Implications for the Hector Mine Event

Our preferred dynamic model for the Hector Mine earthquake is not designed to provide any sort of waveform match to the actual event; far more heterogeneous stress drop and earth structure would clearly be needed to match details of the rupture propagation, slip pattern, and ground motion. However, our preferred model can still be compared to the general features of slip inversions (e.g., Ji *et al.*, 2002; Kaverina *et al.*, 2002) for this earthquake. The total seismic moment of our preferred model is 5.8×10^{19} N m, which is close to the results of Jónsson *et al.* (2002) (5.9×10^{19} N

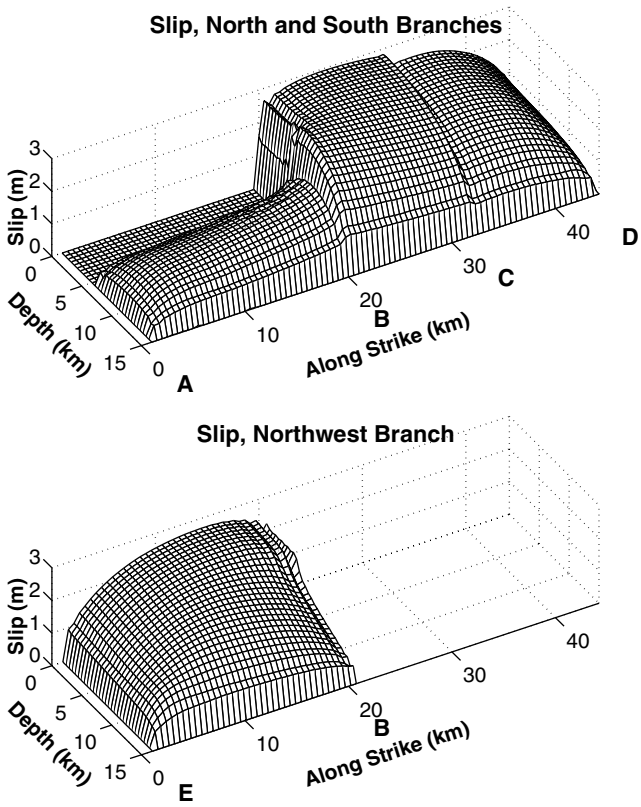

Figure 9. Final modeled slip distribution for the model in which the rupture stops 5 km from the free surface on the north branch. Locations corresponding to A–E on Figure 2a are marked. The slip distribution is similar to that of the preferred model (Fig. 7c), but with smaller slip on the northern part of the north branch.

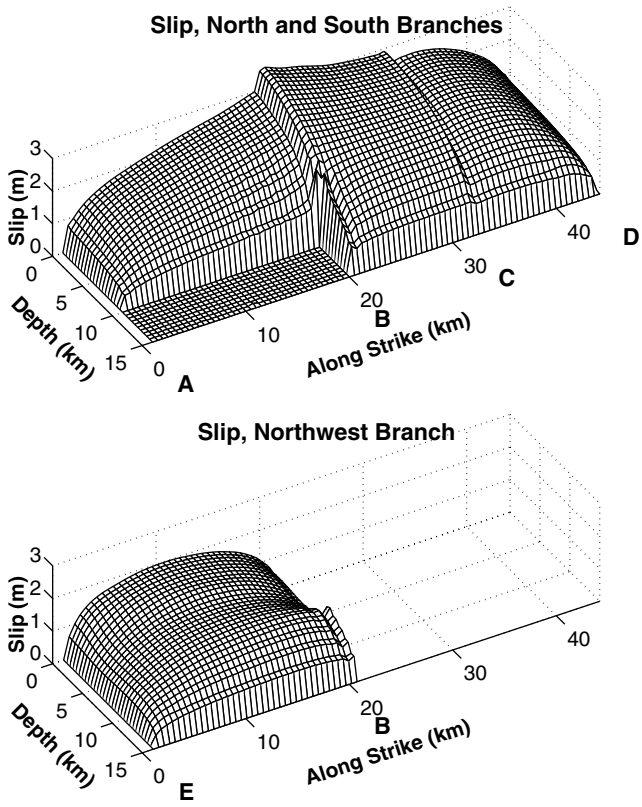

Figure 10. Final modeled slip distribution for the model in which the rupture stops 5 km from the deepest extent of the north branch. Locations corresponding to A–E on Figure 2a are marked. Rupture proceeds to the northwest branch in this model, although the slip distribution is significantly different from that of the preferred model (Fig. 7c).

m) and Ji *et al.* (2002) (6.3×10^{19} N m) and slightly less than the results of Kaverina *et al.* (2002) (6.8×10^{19} N m) and Simons *et al.* (2002) ([6.7–7.2] $\times 10^{19}$ N m). The distribution of the seismic moment in our models also has similarities with Ji *et al.* (2002) and Kaverina *et al.* (2002): all our models have higher slip on the northwest segment than on the north segment north of the junction. In our case, this difference can be explained by the fact that our north segment does not rupture to the free surface, meaning that slip is pinned at the top of the fault, driving slip down over its entire area. Kaverina *et al.* (2002) provided another explanation, determining that the northwest branch had a higher stress drop (by over a factor of 2) than the north branch. Our stress drop is also somewhat higher on the northwest branch, but not nearly as significantly as that of Kaverina *et al.* (2002). An important difference between our dynamic slip pattern and those of the two slip inversions is that both of the inversions have their peak slip on the northwest branch, whereas our peak slip is on the central region of the fault, south of the junction. Therefore, it is difficult to argue that the fault geometry (which is the main feature in our dynamic model) alone is responsible for the relative amount of slip on the different segments. However, our model does strongly argue that the presence of slip on the northwest branch can be attributed to both the combination of fault geometry and the lack of slip on the shallow part of the north branch.

The timing of rupture in Ji *et al.* (2002) and Kaverina *et al.* (2002) also present areas of similarity and areas of conflict with our model. Both these studies note the low (~2.2 km/sec) rupture velocity in this event. Both studies also note that rupture velocity was especially low (~1.8 km/sec) on the north and northwest branches. While our model has higher velocities on the north and south branch (3 and 2.8 km/sec, respectively), the rupture velocity on the northwest branch is only 2 km/sec. Kaverina *et al.* (2002) attributed this slow velocity to greater relative fault strength in this area. In other words, they postulated that the quantity $S = \sigma_y - \sigma_0/\sigma_0 - \sigma_f$ is larger for this branch, where σ_y is the yield stress, σ_0 is the initial shear stress, and σ_f is the sliding frictional stress (Das and Aki, 1977). The yield and sliding frictional stresses are both proportional to the normal stress through the static and dynamic coefficients of friction, respectively. They argued that variations in S are likely to be due to variations in either yield stress or initial shear

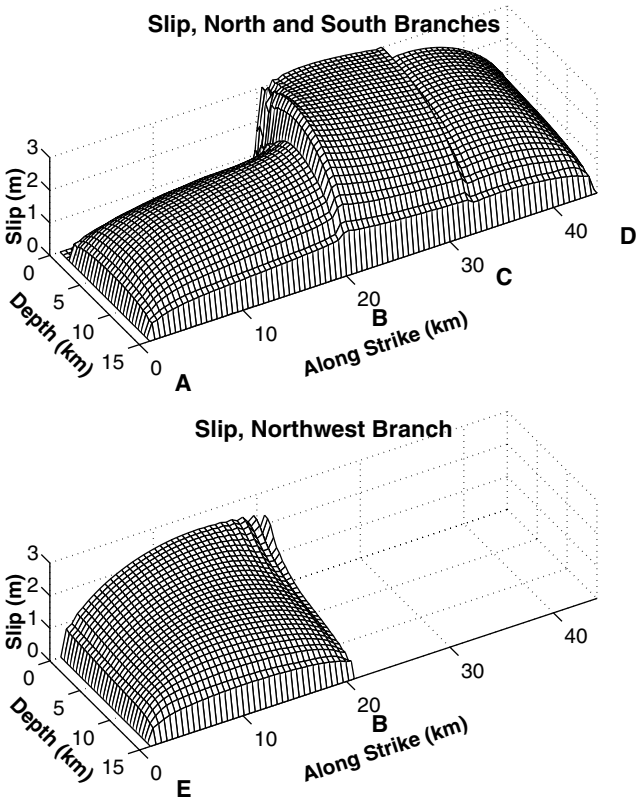

Figure 11. Final modeled slip distribution for the model in which rupture nucleates on the stem of the fault system, south of the branch junction. Locations corresponding to A–E on Figure 2a are marked. The slip distribution is almost identical to that of the preferred model (Fig. 7c), showing the insensitivity of the results to hypocentral location.

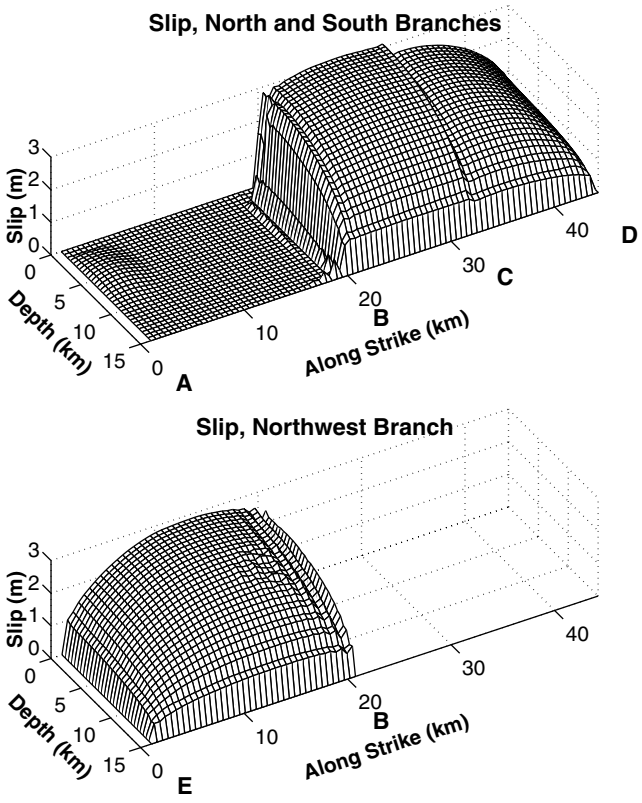

Figure 12. Final modeled slip distribution for the model in which rupture nucleates on the northwest branch. Locations corresponding to A–E on Figure 2a are marked. In this model, rupture barely propagates to the north branch.

stress. Due to our choices for the stress field described in the Methods, our model also has higher S on the northwest branch ($S = 0.72$) than on the north segment ($S = 0.33$). However, the important quantity for rupture of the northwest segment is not the initial S, but S immediately before it ruptures. At this time (shortly before 5.2 sec), S is heterogeneous on the spatial scale of the segment length (i.e., smaller near the surface in the branching region and larger elsewhere, reflecting the stress heterogeneity seen in Fig. 6), with an average value of 1.04. Thus, our model, with its low rupture velocity on the northwest branch, is partially consistent with both waveform inversions. The model explains this anomalously low rupture velocity as being due to a combination of the angle of this branch with respect to the tectonic stress field and its location largely in the stress shadow of the remainder of the fault system. However, our model has larger rupture velocity on the north branch than either slip inversion. It is not clear how to reconcile this disagreement, although it is possible that in the slip inversions, the larger slip on the northwest branch may dominate the solution, leading to less resolution of rupture velocity on the north branch. Alternatively, the north branch may simply have been farther from failure (larger S), rougher, or had a higher fracture energy than our simple model, leading to slower rupture propagation on that branch.

Of course, a large increment in the stress field on the northwest branch is only possible if it ruptures somewhat later than the nearby branches. On this point our work appears to disagree with that of Kaverina *et al.* (2002). Their model (which has nucleation at the segment junction) implies that the north and northwest segments ruptured essentially simultaneously. In contrast, our model has a delay of 5.2 sec between nucleation on the north branch and the onset of slip on the northwest branch. The corresponding delay for our model that nucleates on the stem is 4.5 sec, and for the model that nucleates on the junction, it is 4.6 sec. Our results are more consistent with those of Ji *et al.* (2002), who had a delay of 2–3 sec between nucleation and the onset of rupture on the northwest branch. The location at which rupture begins on the northwest segment is also different between the two waveform inversions and our dynamic models. The model of Ji *et al.* (2002) showed rupture propagating to the northwest branch at a depth of approximately 15 km (near the same depth as their hypocenter), while in Kaverina *et al.* (2002) the corresponding depth was somewhat shallower, but still buried. Our model, however, requires rupture to

jump to the northwest segment very near the surface (as will be discussed in the next subsection). It is not clear, however, how sensitive the final inverted results are to the depth at which rupture jumps to the northwest segment (D. S. Dreger, personal comm., 2002). Thus, our dynamic result for the jump location may be consistent with the strong ground motion, but it is not clear at this time.

Implications for General Fault Dynamics

One of our key results is that the propagation of rupture and slip to the northwest segment can be attributed to a combination of the branched fault geometry and the lack of surface slip on the north fault segment. A stress distribution that leads to zero slip in this area naturally leads to rupture propagation and slip on the northwest branch, whereas stress distributions that lead to shallow slip on the north branch preclude slip on the northwest branch. Similar behavior has been seen in models of overlapping thrust faults (Oglesby *et al.*, 2003). This general conclusion about the Hector Mine event has been made in the preliminary work of Li *et al.* (2002b), but the improved fault geometry, stress distributions, and comparison models used in the current work help to show that this result is not sensitive to the finely tuned details of the faulting model, such as the precise stress distribution or location of the hypocenter. The current study also shows that a time-dependent coulomb stress analysis can help in the prediction and interpretation of the complicated stress interaction leading to rupture propagation on the northwest branch. We find that most of the northwest branch (which overlaps the slipping region of the north branch) is brought farther from failure (with a negative ΔCFS) during the first 5 sec or so of the Hector Mine event. However, the near-surface area that does not overlap with the slipping region of the north branch is brought closer to failure in this same time period. This general effect could be seen even in a static stress transfer analysis, as evidenced by the final frame of Figure 7. However, as is shown in Oglesby *et al.* (2003), when there is a strong two-way interaction between nearby fault segments, a static stress transfer analysis can sometimes give very misleading results as to the ability of rupture to jump from segment to segment, so the ability of a static stress analysis to predict the behavior of such a complex fault system should not be overstated.

An important feature of the preferred model is that rupture jumps to the northwest branch near the free surface. In our preferred model, the primary reason the jump takes place at the surface is that this is the region brought closer to failure by the slip pattern on the north branch. Other models, in which the north branch is constrained not to slip at depth, show that a similar effect can be obtained far from the free surface. However, it is more difficult to achieve this effect at depth, as evidenced by the much larger nonslipping region required at depth on the north branch. Models in which the stress drop tapers to zero within the top 1 km of the model still produce results similar to those of our preferred model, showing that the results are not very sensitive to our simplified assumptions of constant stress drop and frictional properties with depth. The offset/parallel fault models of Harris and Day (1999) also imply that rupture jumps more readily between faults near or at the free surface when the stress drop and frictional characteristics are constant with depth. In our case, one possible reason that the free surface aids rupture jumping is that we have higher slip near the free surface on the stem region. Thus, the slip heterogeneity (strain) near the unslipped surface region of the north branch is high, leading to high stress buildup on the northwest branch. Conversely, we have lower slip at depth, leading to smaller stress increments on the northwest branch in the corresponding models with no slip at depth on the north branch. Additionally, reflected waves from the surface could greatly increase the dynamic interaction between the fault segments near the surface. Nonetheless, the effect at depth could be responsible in other faulting scenarios, in which both branches slip at the free surface. The branched structure at the southern end of the Hector Mine fault system (which we do not model in the current work) is a possible example.

It is useful to interpret the current results in the context of the extensive work on branched fault systems by Kame *et al.* (2003). In their 2D dynamic models of fault systems, they found that the dynamic interaction between fault branches made backward branching (in which rupture starts on one branch, then proceeds on the main fault past the branch point before propagating to the second branch) very difficult for small branching angles. However, our 3D models of the Hector Mine event actually require backward branching for the stress interaction to produce rupture on the northwest branch. This result does not contradict Kame *et al.* (2003). When we allow rupture to proceed to the free surface on the north branch, we obtain results very similar to those of Kame *et al.* (2003): rupture does not propagate to the northwest branch. It is only when we introduce a 3D variation in stress that we obtain slip on both branches. The overlapping thrust fault geometry of Oglesby *et al.* (2003) requires a similar 3D effect to produce jumping rupture. Such 3D effects are not captured in the 2D models of Kame *et al.* (2003), rather, their results help to explain why our models without 3D effects (where rupture proceeds to the free surface on the north branch) do not produce jumping rupture.

A few final points can be made concerning the relationship between the static and dynamic stress fields in these models and other models with nontrivial fault geometry. As noted in the Results, the stress interaction between different fault segments leads (in both the northern and southern sections of the fault system) to slip that is different from what one would have obtained if the various branches had ruptured in isolation. Thus, the prestress level on each segment, while crucially important in determining the final slip of the whole system, is not the only (or perhaps even the most important) factor in determining the final slip on that segment. Also, it is important to note that even in our preferred model, with slightly heterogeneous stress near the free sur-

face, our prestress fields are largely homogeneous prior to rupture. After the fault has slipped, however, the resultant stress field is highly heterogeneous, with strong stress buildups near the geometrical discontinuities (see the final frame of Fig. 6). Qualitatively speaking, the postevent stress heterogeneity in our models consists of rather sharp peaks and troughs on otherwise smooth stress patterns. The fate of these stress peaks and troughs over the interseismic period or multiple earthquake cycles is not at all clear: they could potentially be leveled off by viscoelastic relaxation, aftershocks, creep, or slip on subsidiary/conjugate faults (Andrews, 1989). It is also not clear whether stress heterogeneity will eventually spread to a wider range of length scales. However, it is likely that stress heterogeneity will have an effect in subsequent events on this fault system. If they do not experience great aseismic relaxation, these geometry-induced stress buildups could potentially be even more important than the ambient tectonic stress in determining the behavior of rupture at the segment boundaries. The investigation of features such as these over multiple earthquake cycles is the subject of ongoing work.

Conclusions

We model the dynamics of the 1999 Hector Mine earthquake with a range of assumptions about prestress pattern and hypocenter location. We find that models in which there is no shallow slip on the north branch naturally produce slip on the northwest branch. Other models, in which the north branch slips at the surface, do not produce slip on the northwest branch. Thus, we find a simple stress- and geometry-related explanation for slip on the northwest branch, which upon superficial analysis would appear to be in the stress shadow of the north branch. We also find that a combination of geometrical and stress interaction effects help to explain some additional observed features of this event, such as slow rupture propagation on the northwest branch. The results reinforce our understanding that the geometry of branched fault systems can have a fundamental impact on the patterns of rupture and slip on these systems. Unfortunately, our models show that in some cases, knowledge of fault geometry alone is not sufficient to predict the general behavior of a fault system; the unknown factor of stress heterogeneity can play a crucial role and interact strongly with the fault geometry. Dynamic models of potential future events must include realistic fault geometry, but they must also include many examples of heterogeneous stress fields to capture potential variability in rupture and slip behavior.

Acknowledgments

The authors gratefully acknowledge many helpful conversations with Renata Dmowska, James Rice, and Harsha Bhat concerning fault branching. We also thank Doug Dreger for many useful discussion on the Hector Mine Event. The manuscript was also much improved through helpful reviews by Ruth Harris and Brad Aagaard. Support for this research was provided by USGS Grant Number 02HQGR0009 and by the Dam Safety Program of the U.S. Bureau of Reclamation under project SPVGM.

References

Aagaard, B. T., T. H. Heaton, and J. F. Hall (2001). Dynamic earthquake ruptures in the presence of lithostatic normal stresses: implications for friction models and heat production, *Bull. Seism. Soc. Am.* **91,** 1765–1796.

Andrews, D. J. (1976). Rupture velocity of plane strain shear cracks, *J. Geophys. Res.* **81,** 5679–5687.

Andrews, D. J. (1989). Mechanics of fault junctions, *J. Geophys. Res.* **94,** 9389–9397.

Aochi, H., and E. Fukuyama (2002). Three-dimensional nonplanar simulation of the 1992 Landers earthquake, *J. Geophys. Res.* **107,** ESE 4, 1–12.

Aochi, H., E. Fukuyama, and R. Madariaga (2002). Effect of normal stress during rupture propagation along nonplanar faults, *J. Geophys. Res.* **107,** ESE 5, 1–10.

Aochi, H., E. Fukuyama, and M. Matsu'ura (2000). Selectivity of spontaneous rupture propagation on a branched fault, *Geophys. Res. Lett.* **27,** 3635–3638.

Archuleta, R. J., and G. A. Frazier (1978). Three-dimensional numerical simulations of dynamic faulting in a half-space, *Bull. Seism. Soc. Am.* **68,** 541–572.

Bouchon, M. (1998). Stress field associated with the rupture of the 1992 Landers, California, earthquake and its implications concerning the fault strength at the onset of the earthquake, *J. Geophys. Res.* **103,** 21,091–21,097.

Bouchon, M., and D. Streiff (1997). Propagation of a shear crack on a nonplanar fault: a method of calculation, *Bull. Seism. Soc. Am.* **87,** 61–66.

Das, S., and K. Aki (1977). Numerical study of 2-dimensional spontaneous rupture propagation, *Geophys. J. Royal Ast. Soc.* **50,** 643–668.

Day, S. M. (1982). Three-dimensional simulation of spontaneous rupture: the effect of nonuniform prestress, *Bull. Seism. Soc. Am.* **72,** 1881–1902.

Harris, R. A., and S. M. Day (1993). Dynamics of fault interaction: parallel strike-slip faults, *J. Geophys. Res.* **98,** 4461–4472.

Harris, R. A., and S. M. Day (1999). Dynamic 3D simulations of earthquakes on en echelon faults, *Geophys. Res. Lett.* **26,** 2089–2092.

Harris, R. A., R. J. Archuleta, and S. M. Day (1991). Fault steps and the dynamic rupture process: 2-D numerical simulations of a spontaneously propagating shear fracture, *Geophys. Res. Lett.* **18,** 893–896.

Harris, R. A., J. F. Dolan, R. Hartleb, and S. M. Day (2002). The 1999 Izmit, Turkey, earthquake: a 3D dynamic stress transfer model of intraearthquake triggering, *Bull. Seism. Soc. Am.* **92,** 245–255.

Hauksson, E., L. M. Jones, and K. Hutton (2002). The 1999 M_w 7.1 Hector Mine, California, earthquake sequence: complex conjugate strike-slip faulting, *Bull. Seism. Soc. Am.* **92,** 1154–1170.

Ida, Y. (1972). Cohesive force across the tip of a longitudinal shear crack and Griffith's specific surface energy, *J. Geophys. Res.* **77,** 3796–3805.

Ji, C., D. J. Wald, and D. V. Helmberger (2002). Source description of the 1999 Hector Mine, California, earthquake, part II: Complexity of slip history, *Bull. Seism. Soc. Am.* **92,** 1208–1226.

Jónsson, S., H. Zebker, P. Segall, and F. Amelung (2002). Fault slip distribution of the 1999 M_w 7.1 Hector Mine, California, earthquake, estimated from satellite radar and GPS measurements, *Bull. Seism. Soc. Am.* **92,** 1377–1389.

Kame, N., J. R. Rice, and R. Dmowska (2003). Effects of pre-stress state and rupture velocity on dynamic fault branching, *J. Geophys. Res.* **108,** 2265, doi 10.1029/2002JB002189.

Kase, Y., and K. Kuge (1998). Numerical simulation of spontaneous rupture processes on two non-coplanar faults: the effect of geometry on fault interaction, *Geophys. J. Int.* **135,** 911–922.

Kase, Y., and K. Kuge (2001). Rupture propagation beyond fault discontinuities: significance of fault strike and location, *Geophys. J. Int.* **147,** 330–342.

Kaverina, A., D. Dreger, and E. Price (2002). The combined inversion of seismic and geodetic data for the source process of the 16 October 1999 M_w 7.1 Hector Mine, California, earthquake, *Bull. Seism. Soc. Am.* **92,** 1266–1280.

Li, Y.-G., J. E. Vidale, S. M. Day, and D. D. Oglesby (2002a). Study of the 1999 *M* 7.1 Hector Mine, California, earthquake fault plane by trapped waves, *Bull. Seism. Soc. Am.* **94,** 1318–1332.

Li, Y.-G., J. E. Vidale, D. D. Oglesby, S. M. Day, and E. Cochran (2002b). Multiple-fault rupture of the *M* 7.1 Hector Mine, California, earthquake from fault-zone trapped waves, *J. Geophys. Res.* **108,** 2165, doi 10.1029/2001JB001456.

Oglesby, D. D. (1999). Earthquake dynamics on dip-slip faults, *Ph.D. Thesis*, University of California, Santa Barbara.

Oglesby, D. D., S. M. Day, and D. R. H. O'Connell (2003). The dynamic and static interaction of two thrust faults: a case study with general implications, *J. Geophys. Res.* (in press).

Poliakov, A. N. B., R. Dmowska, and J. R. Rice (2002). Dynamic shear rupture interactions with fault bends and off-axis secondary faulting, *J. Geophys. Res.* **107,** 2295, doi 10.1029/2001JB000572.

Scientists from the USGS, SCEC, and CDMG (2000). Preliminary report on the 16 October 1999 *M* 7.1 Hector Mine, California, earthquake, *Seism. Res. Lett.* **71,** 11–23.

Sieh, K. E., L. M. Jones, E. Hauksson, K. W. Hudnut, D. Eberhart-Phillips, T. H. Heaton, S. E. Hough, L. K. Hutton, H. Kanamori, A. Lilje, S. C. Lindvall, S. F. McGill, J. J. Mori, C. M. Rubin, J. A. Spotila, J. M. Stock, H. K. Thio, J. A. Treiman, B. P. Wernicke, and J. Zachariasen (1993). Near-field investigations of the Landers earthquake sequence, April to July 1992, *Science* **260,** 171–176.

Simons, M., Y. Fialko, and L. Rivera (2002). Coseismic deformation from the 1999 M_w 7.1 Hector Mine, California, earthquake as inferred from InSAR and GPS observations, *Bull. Seism. Soc. Am.* **92,** 1390–1402.

Toksoz, M. N., R. E. Reilinger, C. G. Doll, A. A. Barka, and N. Yalcin (1999). Izmit (Turkey) earthquake of 17 August 1999: first report, *Seism. Res. Lett.* **70,** 669–679.

Whirley, R. G., and B. E. Engelmann (1993). DYNA3D: A Nonlinear, Explicit, Three-Dimensional Finite Element Code for Solid and Structural Mechanics—User Manual, University of California, Lawrence Livermore National Laboratory, UCRL-MA-1107254 Rev. 1.

Department of Earth Sciences
University of California, Riverside
Riverside, California 92521
(D.D.O.)

Department of Geological Sciences
San Diego State University
5500 Campanile Drive
San Diego, California 92182
(S.M.D.)

Department of Earth Sciences
University of Southern California
Los Angeles, California 90089-0740
(Y.-G.L.)

Department of Earth and Space Sciences
University of California, Los Angeles
Los Angeles, California 90095
(J.E.V.)

Manuscript received 31 January 2003.